Solid State Ionics 442 (2026) 117221

Contents lists available at ScienceDirect

Solid State Ionics

journal homepage: www.elsevier.com/locate/ssi

Synergistic coupling between ionomers and solid acids for modulating the superproton conductivity in composites

Bruno R. de Matos [a,*], Ulrich Schade [b], Ljiljana Puskar [b], Elisabete I. Santiago [a], Fabio C. Fonseca [a]

[a] *Instituto de Pesquisas Energéticas e Nucleares, IPEN-CNEN/SP, São Paulo 05508000, Brazil*
[b] *Institute for Electronic Structure Dynamics, Helmholtz-Zentrum Berlin für Materialien und Energie GmbH, Berlin 12489, Germany*

A R T I C L E I N F O

Keywords:
Ionomers
Solid acids
Hybrid
Composite
Superprotonic
Transition
Conductivity

A B S T R A C T

We present a truly synergistic proton conductor composite material based on the addition of solid acids to ionomers. A method for fabricating an interpenetrating network of cesium hydrogen sulfate (CHS) into Nafion ionic domains was developed. The compatibility of the sulfate ions as well as cesium and proton counterions of both phases resulted in a structure in which the Nafion side chains were anchored into CHS phase resulting in a composite material with unique properties. Nafion side chain dynamics were affected by the CHS phase, whereas the CHS lattice parameter was disturbed by the interaction with the polymer side chains. Nafion-CHS composites exhibited a threefold increase in the magnitude of the proton conductivity as compared to that of Nafion in anhydrous condition.

1. Introduction

Hybrid organic-inorganic composites, as intermediate temperature anhydrous proton conductors ($T \sim 80$–200 °C), are key materials to bridge the gap between hydrated polymers ($T \sim 25$–80 °C) and fragile ceramic conductors ($T \sim 300$–600 °C) [1]. Numerous benefits are found in many electrochemical devices related to the use of anhydrous materials. As compared to hydration-dependent components, dry electrodes exhibit higher performance in supercapacitors and batteries [2], and a larger faradaic efficiency (from 83 to 96%) in fuel cells is reached by increasing the operation temperature above the boiling point of water [3].

When the development of anhydrous proton conductors is concerned there is no single strategy that dictates the advancement of the proton conductivity values at high temperatures (80–250 °C) [4–6]. There are two well-known state-of-the-art materials with the highest anhydrous proton conductivity. One material is a polymer, polybenzimidazole doped with anhydrous phosphoric acid and the superprotonic conductor cesium hydrogen sulfate [7]. Both materials display conductivity values in the range of $\sim 10^{-2}$ Scm^{-1} [7]. In addition, the synthesis of proton conducting polymers, composites and nanoparticles are the focus of development for reaching high conductivity values at high T and zero relative humidity [4–6]. One practical alternative is the immobilization of acids in high thermal resistant polymers. However, the main setback is the leaching out of the acid from the polymer during the fuel cell operation [4]. Another strategy involves the use of macromolecules that contain functional groups able to conduct protons [5]. A composite salt of RNA base containing a mixture of uracil with the acidic surfactant monododecyl phosphate exhibited a high thermal resistance (160 °C), nonetheless the proton conductivity remained of the order of 10^{-4} Scm^{-1}. High proton conductivity values at anhydrous conditions were achieved for zirconium acid triphosphate, 10^{-2} Scm^{-1}. Despite the high conductivity values, the temperature range for the high conductivity is rather limited (25–110 °C) [6].

The promise of anhydrous proton conductors has been attested by proof-of-concept studies that pioneered the use of anhydrous oxo-acidic salts, such as cesium hydrogen sulfate ($CsHSO_4$ – CHS) and cesium hydrogen phosphate (CsH_2PO_4 - CHP) in fuel cells [7]. CHS was tested as electrolyte for proton exchange membrane fuel cells (PEMFC) using reformate hydrogen and liquid fuels (methanol, ethanol) [7,8]. A stable fuel cell operation has been reached at intermediate temperatures (150–160 °C) and anhydrous environment using solid acid-based electrolytes [7,8]. However, the polarization curves exhibited large ohmic drops due to the millimeter-thick electrolyte [7]. The solid acids display a fragile-ductile transition at high temperatures requiring a millimeter-thick solid acid electrolyte layer to attain practical mechanical

* Corresponding author.
E-mail address: brmatos@alumni.usp.br (B.R. de Matos).

https://doi.org/10.1016/j.ssi.2026.117221
Received 12 January 2026; Received in revised form 7 April 2026; Accepted 23 April 2026
Available online 30 April 2026

resistance [7]. This scenario evidences the need for enhanced mechanical and electrochemical properties of the superproton conductor. Thus, exploring highly flexible composites using solid acids as the added inorganic phase in proton conducting ionomer matrices is a promising alternative.

The motivation for selecting ionomers as a polymer host for the solid acids relies on the enhanced thermomechanical properties displayed by the former, such as Nafion, in its alkali neutralized or partially neutralized forms [9]. The thermal stability of the ionic clusters, which is the main feature that governs the properties of such materials, is closely related to an appreciable increase in the alpha transition temperature that rises from 110 °C in the acid form to 240 °C for the Cs^+ neutralized form [9]. This characteristic is fundamental for obtaining materials with suitable properties for operation under severe conditions (high *T* and low *RH*) in fuel cells [7,8]. It is worth noting that Cs^+ ions, being the bridging ions that connect the interactions between the Cs^+ terminated ionomer side chains and the added solid acid, create the possibility for constructing truly synergistic composite conductors [10]. The sharing of Cs^+ ions between both phases may establish unique properties since the Nafion cesium ions will be part of the solid acid crystal lattice and the interplay between the dynamics of Nafion side chains as well as the dynamics of the crystal lattice will promote changes in both organic and inorganic phases of the composite material.

One example of composite material is the one formed *via* coupling interactions between a polymer host and a salt discrete phase in which at least one novel property emerges [10]. The synergy between phases has been pursued by various studies targeting to enhance the mechanical and electrical properties following basically four main strategies: *i*) matching the nanosized particles of the inorganic phase with the nanosized ionic domains of the ionomer, where the surface area-dependent interfacial polarizations play a critical role at enhancing the cohesion energy [11]; *ii*) using *in situ* synthesis methodologies that precipitates the second phase in a preformed free-standing film thereby acquiring a fine control of the dispersed phase distribution within the host matrix and maximizing even further the interfacial cohesion area [11]; *iii*) adding an inorganic phase with relevant proton conductivity [12,13]; CHS, for example, displays an abrupt leap of conductivity from 10^{-6} to 10^{-2} Scm^{-1} at $T > 140$ °C; and *iv*) matching compatible organic-inorganic functional groups, which promotes a high level of interaction, *i.e.*, the surface modified inorganic phase establish a connection with the polymer phase; this latter item modifies profoundly the resulting properties of the composite material and remains largely underexplored [14]. In the case of polymer / solid acid composites, such matching can be reached due to the chemical affinity between RSO_3Cs (Nafion) and $CsHSO_4$, in which both ionomer and the added nanophase will have its properties modified after the mixture takes place, resulting in a material with new properties not inherited from the individual phases. It is interesting to note that at anhydrous condition there will be a strong binding between sulfates from the organic and inorganic phases and the energy associated with the segmental motions of the main and side chains of the ionomer may exert a pull on the crystal lattice of the CHS. This phenomenon is virtually not observed in several ionomer-based composite materials that utilize nanoparticles with large lattice energies, such as titanates (−12,000 $kJ.mol^{-1}$), silicates (−13,000 $kJ.mol^{-1}$), zirconates (−9700 $kJ.mol^{-1}$), *etc.* [15–17].

Furthermore, the ionomer side chains being bridged with the inorganic phase *via* Cs^+ and H^+ ionic and hydrogen bond interactions may have a strong influence on the superprotonic phase transition of the CHS and CHP phases [18]. The superproton conduction of CHS is assigned to the high atomic number of Cs^+ — the HSO_4 tetrahedra vibrates against large Cs^+ promoting large vibrations amplitudes and consequently weakens the electrostatic bonds facilitating the proton migration [19,20]. Hence, the search for synergistic composite materials is very promising due to the possibility of tuning the superprotonic conductivity transition.

It has been reported the importance of sustaining a continuous nanostructure of an ion conducting path for reaching high levels of proton conduction [21]. The addition of fillers into an ionomer matrix may disrupt the ionic network continuity and cause a reduction of the mechanical strength of the polymeric membrane [22]. The addition of polymer like quantum dots into Nafion was shown to promote a molecular-level hybridization due to a match of size scales, which resulted in an improved ion conduction network and, as such, a higher proton conductivity value with respect to pristine Nafion [23]. However, despite the higher conductivity, it is highly dependent on humidity, otherwise being an insulator in the absence of water.

Herein, we developed a method for obtaining synergistic composite materials *via in situ* precipitation of solid acids, cesium hydrogen sulfate nanoparticles, into a sulfonated ionomer matrix, Nafion. The biggest challenge was producing Nafion-$CsHSO_4$ composites with high concentration of the inorganic phase surpassing the percolation threshold. This issue was solved by a two-step synthesis in which the Nafion matrix was irreversibly expanded *via* thermal annealing at high relative humidity, allowing the incorporation of solid acids above the percolation threshold. Such result allowed for the elevation of the proton conductivity by three orders of magnitude under anhydrous conditions when compared to unfilled Nafion. The ion conductivity follows the VTF temperature dependence confirming the ion transport modulation with the main and side chain motion of Nafion.

2. Experimental

2.1. Preparation of the hybrid organic-inorganic composites

The composite membranes of Nafion with addition of $CsHSO_4$ (CHS) were prepared by *in situ* evaporation/precipitation method [15]. Samples of Nafion + *x* CHS, labelled N-CHS*x*, were prepared for $x = 11$ vol%, 17 vol% and 28 vol%. Commercial Nafion membranes (N115 - $EW =$ 1100 g Eq^{-1}) were obtained from DuPont. N115 samples were placed over millimeter sized zirconia spheres in a Teflon container. The role of the zirconia spheres was to allow the film to be fully immersed in the precursor solution facilitating the access to whole film surface and as well as avoiding the attachment of the film to the casting mold.

Three procedures were used to prepare the composite samples with different volume fractions of the solid acid. In the first, the composite materials were prepared using water as solvent. The N-CHS prepared in water was initially swollen in 80 mL of a $CsHSO_4$ aqueous solution for 1 h. The next step consisted of positioning the casting mold in a resistive furnace at $T = 120$ °C for 6 h for the evaporation of water and precipitation of the inorganic phase. This procedure allows the preparation of N-CHS samples with the concentration of ~10–12 vol% of the $CsHSO_4$. The second procedure consisted of using dimethylsulfoxide (DMSO) as solvent, this modification was found necessary because it swells Nafion membranes (~ 77 wt%) much more than water. Thus, DMSO solvent allows a higher penetration of the solid acid precursor solution into the polymer film to reach higher volumetric fraction aiming at the percolation threshold of the inorganic phase. Taking the theoretical threshold for an ideal binary composite (a continuous host matrix containing discrete spherical particles) as a reference, the percolation threshold is *c* ~ 15 vol% [23]. Empirically the percolation threshold for Nafion-Silica and Nafion-Titania composites revolves around 13–16 vol% [15,25]. In order to prepare highly concentrated samples, the following procedure was employed. The N-CHS was prepared by immersing N115 in 40 mL of a $CsHSO_4$ aqueous solution for 1 h; subsequently, the concentration was reduced by half after the addition of DMSO to the mold. The evaporation step was performed by placing the casting mold in a resistive furnace programmed at two drying ramps, the first at $T = 130$ °C for 24 h – for the evaporation of the DMSO solution and precipitation of the inorganic phase –, and the second $T = 160$ °C for 6 h – for the total elimination of any DMSO residues. This procedure leads to the preparation of N-CHS samples with the concentration of ~16–17 vol% of the $CsHSO_4$. The last method followed the same procedure as for the second, with the only modification being in pre-treatment of the membrane. A high relative humidity annealing in Nafion at $T = 140$ °C and $RH = 100\%$, was reported previously to expand the polymer structure irreversibly, allowing the film to absorb double the amount of water as compared to the pristine polymer [26]. This pre-annealing allows the preparation of N-CHS samples with the concentration of ~26–28 vol% of the $CsHSO_4$. After preparation all dried samples were kept in a closed recipient containing silica gel and placed inside a desiccator previous the characterization. The dry composite thickness for all compositions was ~160 μm.

2.2. Preparation of Nafion reference samples

Nafion samples exhibit markedly different electrical properties and structural characteristics when probed by small angle X-ray scattering (SAXS) depending on the ionic form (proton and cesium forms). Thus, in order to distinguish the contribution of the Cs^+ ions to the SAXS patterns of Nafion in the cesium form and the Nafion+$CsHSO_4$ composites, measurements of selected reference Nafion samples were carried out. Three reference samples were prepared: N115 in the H^+ form, N115 in the Cs^+ form, and a Nafion in the form of half mol of H^+ and half Cs^+. N115-H^+ were pre-treated by standard cleaning and activation protocols [26]. The film was then post-treated in 3% (*w*/w) H_2O_2 and 0.5 M H_2SO_4, with intermediate steps in H_2O to remove excess chemicals [26]. The samples in the cesium form were obtained by two successive treatments in 1 M CsCl for 1 h followed by two water washings to remove excess chemicals [27]. Nafion in the mixed form of H^+/Cs^+ was prepared by varying the concentration of CsCl in the solution until half of the protonic charges were replaced by cesium ions. The composition of the sample was confirmed by acid-base titration.

2.3. Small angle X-ray scattering

The samples were examined by SAXS at the Brazilian National Synchrotron Light Laboratory (LNLS) ($\lambda = 1.488$ Å). The scattering intensity (I) *vs* scattering vector, $q = 4\pi \sin\theta\, \lambda^{-1}$ data were collected in the range of $q \sim 0.1$–3.5 nm^{-1}. The scattering patterns were collected with MarCCD detector. The scattering patterns were also corrected for transmission, normalized upon the background scattering before data integration. Additional X-ray diffraction (XRD) measurements were performed using Rigaku-Miniflex II diffractometer with Cuk_α radiation ($\lambda = 1.54$ Å) in the 2θ range of 5–80°.

2.4. Scanning electron microscopy

The microstructure of the surface of the membranes was evaluated using the JEOL JSM-6010LA scanning electron microscope (SEM). The surface of the membranes was recovered with gold sputtering. Image-J software was used to calculate the interparticle distance using SEM images *via* Fast Fourier Transform (FFT). The elemental mapping of fluor and cesium was carried out by energy dispersive X-ray spectroscopy (EDS).

2.5. Fourier transform infrared spectroscopy (mid and far infrared)

The FTIR measurements in both mid and far ranges were combined to evaluate the CHS within the composite membranes. Specifically, the far infrared region permits to obtain information regarding the lattice polarizations of the CHS phase [28,29]. Far infrared (FIR) spectra of films were measured at the IRIS beamline at the electron storage ring BESSY II of Helmholtz Zentrum Berlin. For the spectral region between 600 and 30 cm^{-1} films were measured in transmission mode under vacuum (< 0.1 mbar) of the sample chamber of the Bruker Vertex 70/v spectrometer, using infrared synchrotron radiation and a liquid helium cooled silicon bolometer (FIR) detector. The spectral resolution of 2 cm^{-1} and 128 co-added scans for both sample and the reference were used with the references being taken through the empty channel inside the spectrometer sample compartment. Data acquisition was started when films were sufficiently dry and no further changes in the water-related characteristics could be observed spectroscopically. Additional mid infrared spectra were performed in the ATR mode using a ZnSe crystal with the Nicolet FT-IR 6700 spectrometer. For these measurements, the samples were previously dried and immediately placed inside the instrument. The measurements were performed under room temperature and relative humidity.

2.6. Uniaxial tensile testing

The mechanical properties of the composite membranes were evaluated by stress-strain curves taken in a Stable Micro Systems (model TA. XT/PlusC) at a velocity rate of ~50 mm min^{-1}. Stripes with 10 mm of width and 50 mm of length were cut from the composite samples and tested at ambient conditions (temperature and relative humidity).

2.7. Electrochemical impedance spectroscopy

Electrochemical impedance spectroscopy (EIS) data were collected in a specially designed air-tight sample holder able to measure the proton conductivity in the range $T = 30$–240 °C with $RH = 0\%$ (dry N_2 purge) and with RH ranging from ~0 to 100% [26,27]. Temperature controllers connected to band heaters placed externally around the cylindrical chambers were monitored by thermocouples (type K) inserted inside the metallic walls. Nafion samples were sandwiched between stainless steel spring-load contact terminals (electrically insulated from the chamber walls) with carbon cloth to facilitate water equilibration. In this experimental apparatus, the RH of the sample chamber can be calculated by $RH = \rho(T_r)/P(T_c)\mathrm{x}100$, where ρ is the vapor partial pressure, P is the saturated vapor partial pressure, and T_r and T_c are the water reservoir and sample chamber temperatures respectively. A Solartron 1260 frequency response analyzer was used in the frequency (f) range of 4 mHz to 3 MHz applying an *ac* amplitude of 100 mV [26,27].

3. Results and discussion

Fig. 1a and b show the SAXS plots for the three reference Nafion samples in the H^+, Cs^+ and H^+/Cs^+ forms in dried (Fig. 1a) and hydrated forms (Fig. 1b), and for the prepared composite samples (Fig. 1c). Fig. 1a and b shows the typical SAXS patterns for Nafion in both the proton and cesium forms. Both Nafion samples show the characteristic ionomer peak located at $q \sim 2$ nm^{-1} that displaces to $q \sim 1.0$–1.2 nm^{-1} upon increased hydration. The so-called matrix peak appears at $q \sim 0.6$ nm^{-1} and shifts to $q \sim 0.1$–0.2 nm^{-1} due to water swelling. It was acknowledged that just with the resource of theoretical simulations it was not possible to determine whether the shape of the ionic domains is lamellar or cylindrical [30]. The interpretation of the ionomer and matrix peaks as well as the shape of the ionic and non-ionic domains of Nafion has been under dispute for more than 50 years [31]. More recently it was empirically determined, *via* an intense ordering of the ionic domains of Nafion by electric and magnetic fields assisted casting, that the ionic domains of Nafion assume a lamellar arrangement as confirmed by the lamellar signature reflections in SAXS patterns [31]. Such experimental signatures were shown to be present in the scattering patterns of Nafion in the cesium form as the ones shown in Fig. 1b. The observed SAXS peaks, occurring at q and $2q$, confirm the lamellar arrangement of the ionic aggregates into Nafion in the hydrated form [31]. It is worth noting that the precipitation of the $CsHSO_4$ into Nafion, if it occurs inside the ionic domains, is expected to produce a low-q displacement of the ionomer-peak similar to the ones observed for Nafion upon hydration (Fig. 1b). Such an anticipated inference for the displacement of the ionomer peak is in good agreement with the observed features in the SAXS patterns of the composite samples shown in Fig. 1c.

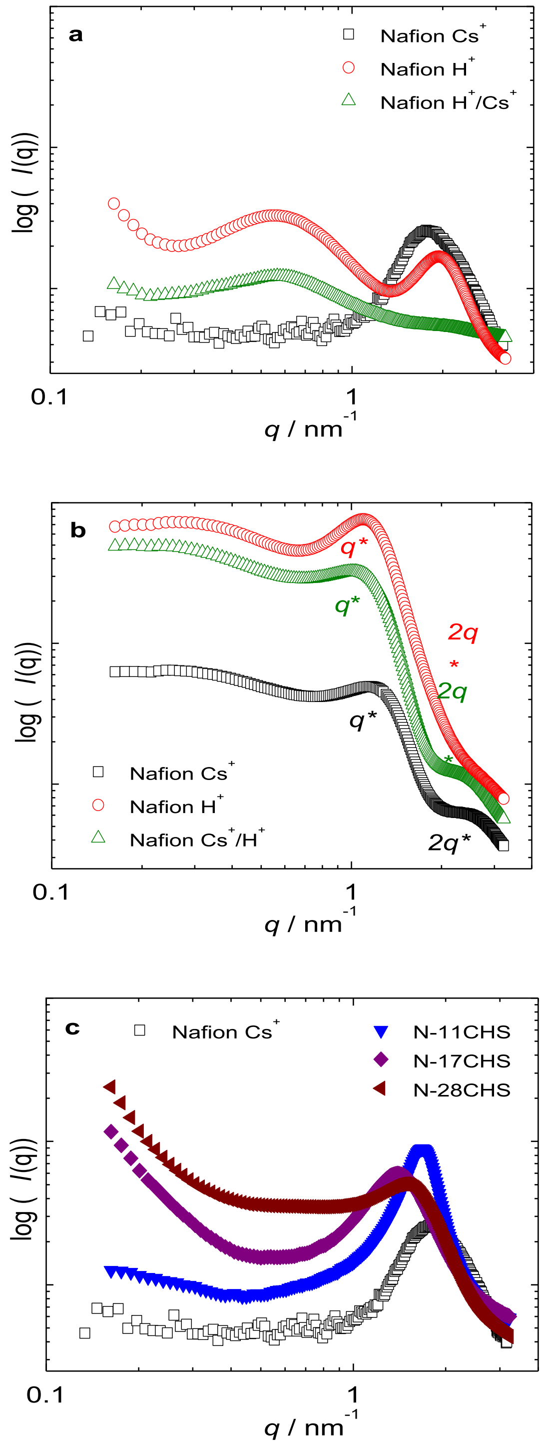

Fig. 1. SAXS patterns for reference Nafion samples, Nafion Cs^+, Nafion H^+, Nafion H^+/Cs^+ in the dry (a) and fully hydrated (b) forms. (c) SAXS patterns for the composites N-CHS with different compositions.

The addition of the inorganic phase increases the intensity and displaces the ionomer peak to lower angles from $q \sim 1.8\ nm^{-1}$ (Nafion Cs^+) to $q \sim 1.68\ nm^{-1}$, $1.38\ nm^{-1}$ and $1.49\ nm^{-1}$ for N-11CHS, N-17CHS and N-28CHS, respectively. The displacement of the ionomer peak to lower angles and the increment in intensity are associated with the *in-situ* growth of the $CsHSO_4$ phase within the clustered ionic domains. It has been reported for Nafion-zirconium phosphate composites that when precipitation of the inorganic phase occurs outside the ionic domains the ionomer-peak position remains unaffected by the incorporation of nanoparticles [12]. In Fig. 1c, the ionomer-peak of N-11CHS is sharper than that of Nafion Cs^+ indicating a more ordered structure for the composite sample. This feature indicates that the $CsHSO_4$ precipitation in the composite prepared using water as solvent exclusively takes place within the ionic domains. This is possibly the reason why the ionomer peak of such composites has higher intensities than the ones prepared with DMSO (Fig. 1c). The scattering curves of N-17CHS and N-28CHS exhibit higher scattering intensities at intermediate ($q \sim 0.4$–$0.8\ nm^{-1}$) and low ($q < 0.4\ nm^{-1}$) q-ranges than N-11CHS, which is in good agreement with the larger volume fraction of the inorganic phase. The higher intensities at intermediate q-ranges may be due to lower scattering contrast if the inorganic phase is not placed preferentially inside the ionic domains and occupies interspace regions among the ionic domains. Evidence that supports this feature is that DMSO solvates both ionic and nonionic domains of Nafion allowing the access of the inorganic phase at distinct regions of the matrix morphology [32]. At intermediate q-range, the N-28CHS sample possesses the highest scattering intensity that is an outcome of the high *RH* thermal annealing used for samples with a higher intake of the added phase. The increased scattering intensities observed at low q-range for N-17CHS and N-28CHS are associated with a long-range network of the $CsHSO_4$ phase existing in the sample. In accordance with the expected volume fraction to reach the percolation threshold of the inorganic phase (> 13–16 vol%), the low-q large scattering intensities is evidence of the percolation of the inorganic phase into the polymer matrix [15,24,25]. It is worth noting that the increase of the scattering intensities at both low and middle q-ranges with the growing network of the inorganic phase suggests that the ionic clusters in Nafion are interconnected *via* channels [33]. Nonetheless, the most important finding for the present investigation concerns the size range of the $CsHSO_4$ phase produced in the interior of Nafion. The SAXS patterns show that a $CsHSO_4$ nanophase is distinguished in the matrix morphology. According to the $d = 2\pi q^{-1}$ the dimensions of the $CsHSO_4$ filled ionic domains are 3.74, 4.55, and 4.22 nm for N-11CHS, N-17CHS, and N-28CHS, respectively.

The size of the lamellar ionic domains of Nafion is known to be the result of the sum of the side chain length of the two adjacent ionic aggregates forming the lamella plus the length of the ionic aggregate itself [31]. In the dry form, the SAXS measurements indicate that the size of such lamella for Nafion-Cs^+ is $d \sim 3.49$ nm (Fig. 1a) and the composite morphology is therefore composed of a $CsHSO_4$ phase embedded in this lamellar arrangement of the ionic clusters of Nafion. In this arrangement SO_3H^+/SO_3Cs^+ clusters are an integrant part of the nanoparticle composition and suggests that the lamellar array of the ionic clusters serves as a template for the growth of the $CsHSO_4$ phase.

In order to assess the morphology of the composite membranes, SEM-FEG measurements were performed and shown in Fig. 2.

Fig. 2a, b and c shows the SEM-FEG images of the surface of Nafion, N-CHS11 and N-CHS28, respectively. It can be observed in the images that the membrane Nafion and N-CHS11 exhibit a rather smooth and clean surface as compared to the N-CHS28 sample. In the composite N-CHS11 a visible superficial texture evidences a rougher surface as compared to Nafion, while the absence of regions with evident contrast differences, indicates small influence of the added second phase. Differently, the image of N-CHS28 displays easily discernible and homogeneously distributed regions with brighter contrast than the Nafion matrix, corresponding to ridges and microparticles (~ 3–7 μm) embedded in the surface. Such brighter contrast regions are attributed to a partial segregation of the inorganic phase in the surface of the Nafion matrix in the sample with the highest volumetric fraction of CHS. The observed features revealed by the FEG analysis reflect the bulk properties of the composite samples and confirm that the N-CHS28 sample reaches a concentration of the inorganic phase in which significant changes take place.

In order to confirm the chemical composition of the microparticles observed in N-CHS28 surfaces, the EDS mapping of fluor (only existing within the polymer phase) and the cesium (existing in both polymer and

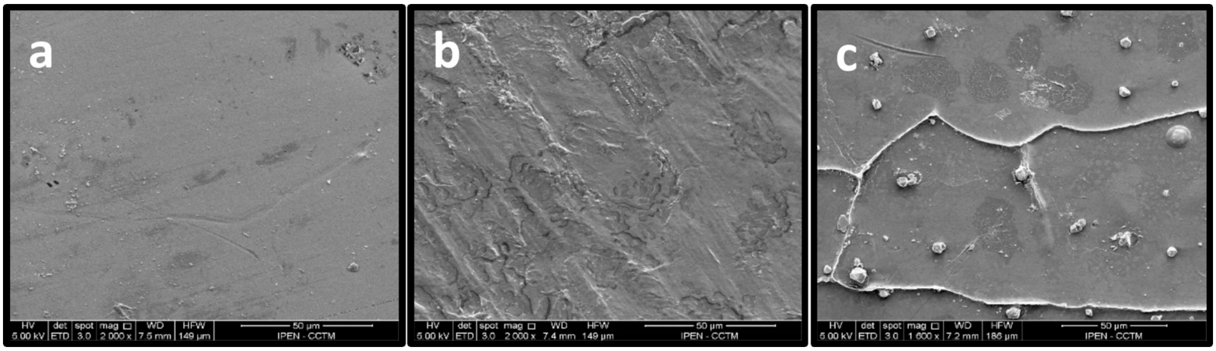

Fig. 2. SEM-FEG microscopy images of Nafion (a), N-CHS11 (b) and N-CHS28 (c).

particle phases) are shown in Fig. 3.

By comparing the SEM-FEG images and the EDS mapping of the samples with no surface modification, Nafion (Figs. 3a to 3c) and N-CHS11 (Figs. 3d to 3g), with the ones obtained for N-CHS28 (Figs. 3g to 3i), it is possible to infer that the homogeneously dispersed particles are mainly associated with the CHS phase. Such regions are possibly related to the measured upturn of the SAXS data at low-q observed in the scattering patterns of N-CHS28 sample (Fig. 1c). Low magnification images of N-CHS28 sample (Figs. 4a and 4b) reveal that these microparticles are ubiquitously observed throughout the sample surface. The Fourier Transform of Fig. 4b, shown in Fig. 4c, displays two characteristic spectral features: an outer and inner haloes. The broad outer halo is associated with the characteristic sizes in the ~2.5–5.0 μm range. The combined SEM-FEG and EDS analyses evidence that there is a long-range arrangement of cesium hydrogen sulfate microparticles on the membrane surface, as the inner halo observed in the FFT image indicates an average interparticle spacing of ~20 μm.

It is interesting to notice that the arrangement of CHS particles in Nafion reflects the employed synthesis method. Because the *in situ* synthesis of the CHS phase uses the Nafion morphology as a template to guide the growth of the particles, the evidence of a correlation length existing among the microparticles shows that the CHS crystals follow the matrix template and are embedded in a pre-existing long-range ordering of the ionic aggregates in the Nafion matrix [34,35].

Fig. 5 shows the XRD patterns for Nafion, $CsHSO_4$ powder, and the composite samples. The XRD data of Nafion samples display two haloes placed at $2\theta \sim 16$ and 40° assigned to reflections arising from the amorphous domains of Nafion (Fig. 5). Such halos are significantly

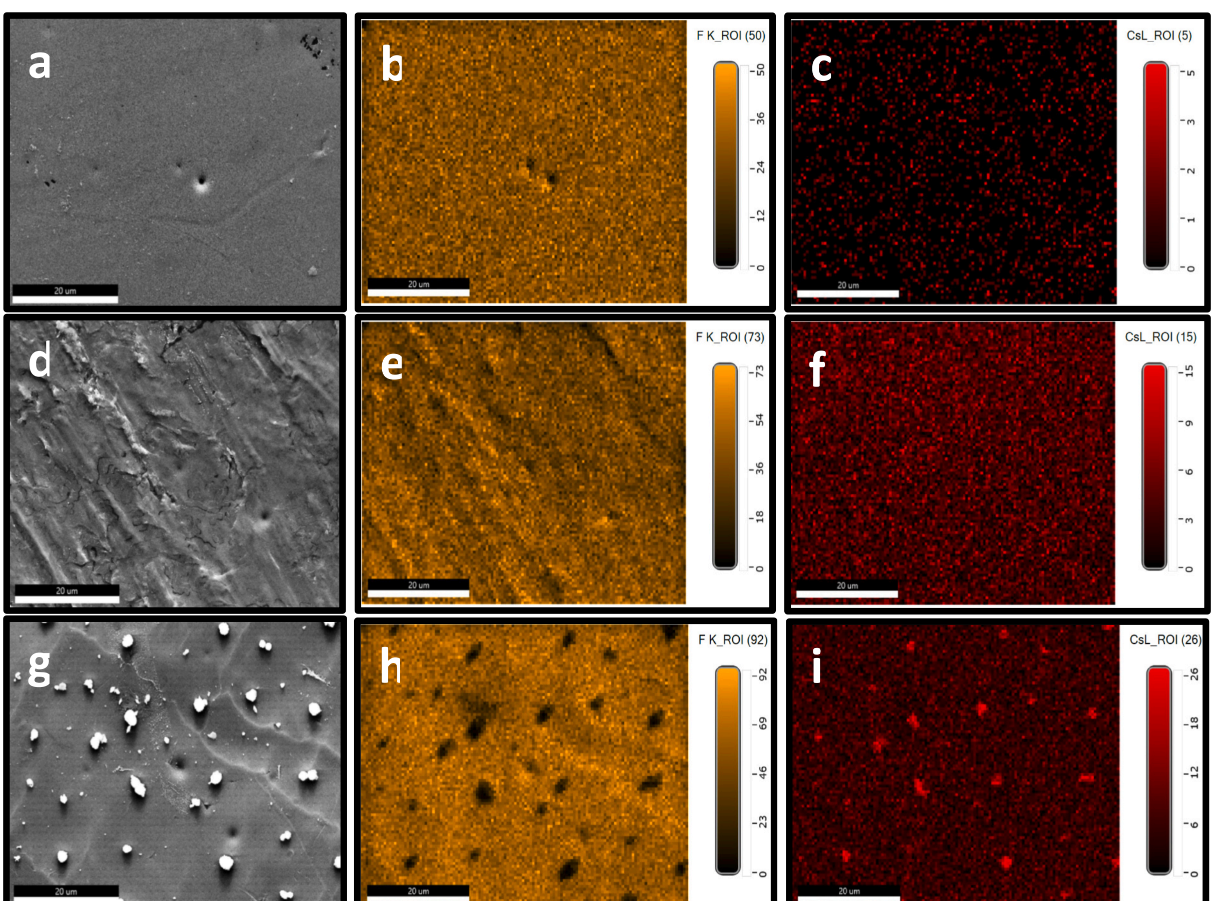

Fig. 3. SEM-FEG images of Nafion (a), N-CHS11 (d) and N-CHS28 (g), and their respective EDS mapping of fluor (b, e and f) and cesium (c, f and i).

suppressed in the XRD patterns of the composite samples. The XRD pattern of the $CsHSO_4$ exhibits maximum relative intensity reflections of the CHS at $2\theta \sim 25^\circ$, 28°, and 32° indicating the phase II of monoclinic CHS $\lesssim P2_1/c \gtrsim$, in perfect agreement with previously reported data [19]. Interestingly, the XRD patterns of the composite samples N-11CHS and N-17CHS exhibit a broad halo in the same $2\theta \sim 25^\circ$, which is likely to be due to the $CsHSO_4$ nanophase in the ionic domains of Nafion. In accordance with the SAXS analysis, the XRD patterns of the composite materials reveal a tendency of the $CsHSO_4$ to crystallize. However, such small nanoparticles under the influence of the disturbance of side chains possibly impairs more extensive crystallization and coalescence of CHS particles. The XRD data indicates a high degree of interaction of Nafion and an inhibited ordering of the Cs^+, H^+ and the SO_4^- counterions. According to SAXS analysis the CHS phase size is in the range of an expanded ionic clusters of ~4 nm which impedes the observation of well-defined XRD reflections. Moreover, the microparticles analysis existing at the composite surface identified in SEM-FEG possibly does not produce sufficient signal-to-noise ratio to turn evident the characteristic peaks of the CHS phase.

Further analysis of the composite materials was performed by FTIR (Fig. 6). Owing to the similarities of the vibrational bands found for SO bonds in both $CsHSO_4$ and in the side chain terminal groups of Nafion, RSO_3H, an overlap of these bands is observed, impeding a detailed analysis of the vibrational bands of the composite samples. In Fig. 6a and b, the mid-infrared range (ATR mode) spectra of N-CHS confirmed the presence of vibrations associated with hydrogen bonding stretching in CHS, which are reported to be located at ~2850, 2535, 2485, and 1708 cm^{-1} [35]. Such bands are observed in the spectra of N-28CHS and it is less discernible for N-11CHS, as shown. Possibly, due to the lower amount of the inorganic phase in the sample the intensity of the CHS phase is reduced with respect to the absorption bands of Nafion. Moreover, in Fig. 6b, two fundamental vibrations observed at 1023 and 862 cm^{-1} can be promptly identified for N-28CHS but are absent in the Nafion spectra. Such bands further confirm the incorporation of the CHS phase into Nafion. In Fig. 6b, the 1055 cm^{-1} band observed in Nafion spectrum, attributed to the SO stretching of Nafion side chains, displaces to 1050 cm^{-1} for N-11CHS. For N-28CHS this displacement is so large that the band merges with the low-frequency band of CHS inhibiting the peak determination. Displacements of the order of 5 to 10 cm^{-1} are observed for the 1055 cm^{-1} band, assigned to the symmetric stretching vibrational mode of the Nafion sulfate group (νSO), for increasing the sample water content, and it occurs due to changes in the surrounding environment of SO_3H groups by the presence of water [36]. In the lithium form of Nafion, a displacement from 1073 to 1058 cm^{-1} with increasing water sorption was reported [36]. The main cause for such shift has been attributed to the polarization of the S—O dipole by the neighboring counterions in the dry state [36]. As such, the low-wavelength shift with increasing CHS content may be assigned to the presence of a higher amount of water in the composite containing the highest amount of CHS. This evidence is backed up by the high relative intensity of the bending band of water located at ~1650 cm^{-1}, as well as the high relative intensity of the 980 cm^{-1} band with respect to the 970 cm^{-1} band observed for N-28CHS. However, the broadening of the νSO band could be attributed to the surrounding CHS phase within the ionic clusters since upon hydration the peak width at half height decreases [36].

In Fig. 6c and d, the far infrared spectra of the samples studied are presented. Since these measurements were performed with the sample kept under vacuum, the observed features arise mainly because of the composite sample composition. The spectra of Nafion in the cesium form contain distinguished absorptions bands at 203 cm^{-1} and 100 cm^{-1}, which are assigned to the CF_2 stretching and the cation motion, respectively [31,37]. The composite spectra consist of these two Nafion bands overlapped with the CHS bands appearing in the region of 480–378 cm^{-1} that can be assigned to the deformations of the S-OH bond (Fig. 6c) [28,29,38]. In addition, the low-frequency band located at 190 cm^{-1} is possibly associated with rotational vibrations of HSO_4^{2-} anions strongly involved in hydrogen bond stretching, whereas the four bands observed in the lowest frequency range placed at wavenumbers < ~ 100 cm^{-1} are attributed to lattice resonant vibrations associated with the motion of Cs^+ cations [28,29,38]. It is worth noting that high frequency displacements of these four bands are seen with increasing CHS relative volume fraction. It is possible that as the CHS content increases, the phase becomes bulkier and the displacement reflects the stronger bonds in a more ordered CHS phase. These features are in excellent agreement with the SEM-FEG analysis that showed bulkier microparticles for N-CHS28 (Fig. 4). As such, it suggests that for the composites N-11CHS and N-17CHS, there is a higher influence of the anchored side chains in the structure causing a possible disordering of the CHS phase, while as the CHS phase becomes bulkier in the N-28CHS, the properties of the CHS become more evident.

Such scenario for the synergistic interactions between the organic and inorganic phases is promoted when considering the electrostatic attraction among the ionic groups terminated side chains and the CHS phase. It was defined that the electrostatic work necessary to disrupt the ionic aggregate is proportional to the polymer T_g: $T_g \propto W_{el} = \int \frac{q_a q_c}{a^2} da \propto \frac{q_a q_c}{a}$, where a is the lattice constant [21]. Such dependence evidences the direct influence of the polymer T_g on the lattice parameter of the ionic aggregates attached in the CHS phase.

Fig. 7 shows the stress-strain curves of Nafion and the NCHS composite samples. The measured Young's modulus of Nafion is ~162 MPa, which is in good agreement with reported values [39,40]. The addition of 11 and 28 vol% of the inorganic phase resulted in an increase of the Young's modulus to ~353 GPa and 480 MPa, respectively. This finding evidences an improvement of the mechanical properties after the incorporation of the CHS phase into Nafion. It is interesting to notice that the composite material developed a more defined transition between the linear elastic modulus region from the yield strength showing a maximum in the stress-strain curve. This behavior represents a higher resistance towards plastic deformation due to the incorporation of CHS phase into the polymer. The stress-strain maximum is found at ~26 MPa and at ~42 MPa for N-CHS11 and N-CHS28, respectively, representing a significant enhancement of the mechanical strength with respect to Nafion.

In Fig. 8a, the ionic conductivities of the reference samples are shown. The ionic conductivity measurements of Nafion samples in anhydrous conditions are rare. The previously reported data were collected within a very limited temperature range (30–120 °C) [41]. As can be seen in Fig. 8a, the ionic conductivity of Nafion is strongly dependent on the ionic form (H^+, Cs^+). It has been shown previously that the ionic conductivity of Nafion follows the Vogel-Tamman-Fulcher (VTF) temperature dependence in both the proton and alkali forms [9,27]. The magnitude of the conductivity depends on the dynamics of the segmental motions of alpha and beta relaxations of Nafion. The best VTF fit parameters for the conductivity of Nafion-Cs^+ was $E_a \sim 0.25$ eV and a Vogel temperature, T_0 of ~7 °C. It has been reported that the T_g of Nafion cannot be identified *via* differential scanning calorimetry (DSC) experiments [9] and therefore the fitted T_0 values cannot be compared with DSC experiments [9]. However, the VTF fitting of the conductivity and dielectric data of ionomers has been responsible for the best identification of the ionomer T_g in these situations where it cannot be determined by DSC or dynamic mechanical analysis (DMA) [9]. The proton conductivity of anhydrous Nafion-H^+ displays a maximum at $T \sim 120$ °C. The maximum observed in Fig. 8a for Nafion-H^+ represents two VTF-like conductivities in which, the one in the T-range of 40–120 °C is the proton motion modulated by the short-range segmental motion of side chains (β-relaxation) and the later in the T-range of 160–200 °C corresponds to the proton transport modulated by the long-range main chain motion (α-relaxation) [42]. Both VTF segments are fitted with a single $T_0 \sim -125$ °C and $E_a = 0.15$ eV. T_0 is usually 100 degrees lower than the T_g, and the fitted T_0 values for Nafion in the

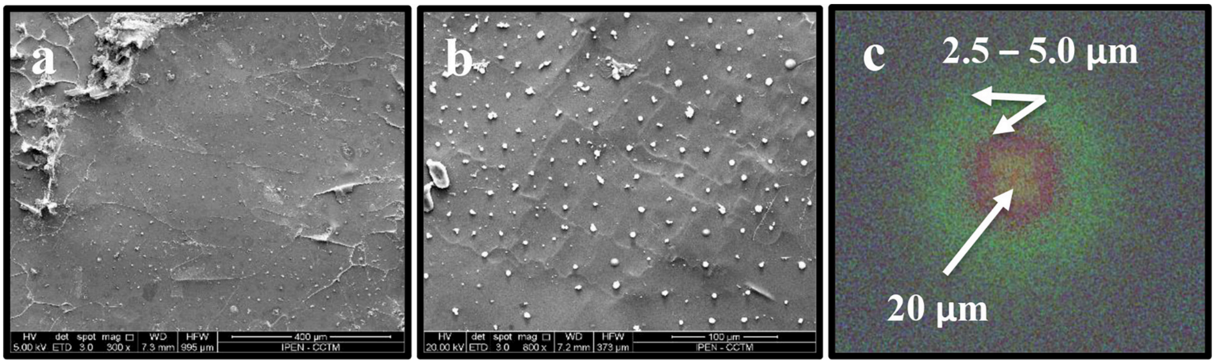

Fig. 4. SEM-FEG images of N-CHS28 at lower magnifications (a and b) and the Fourier Transform of image in b (c).

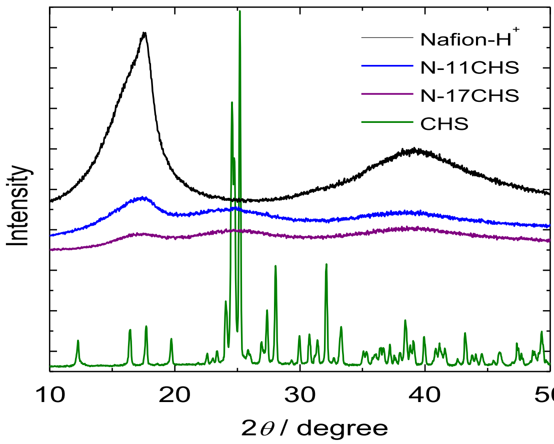

Fig. 5. XRD patterns of the composites N-11CHS and N-17CHS and the reference samples Nafion H$^+$ and CHS.

cesium and proton forms are in excellent agreement with the T_g values reported, $T_g \sim -20$ °C and 130 °C, respectively [9,27]. The mixed H$^+$/Cs$^+$ conductivity displays two VTF dependences at a low (60–120 °C) and high (150–240 °C) T-ranges. The low-T conductivity is fitted with $E_a \sim 0.15$ eV and $T_0 \sim -100$ °C, whereas the high-T conductivity has E_a of

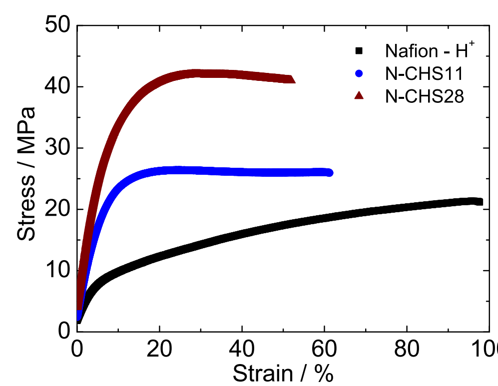

Fig. 7. Uniaxial tensile testing of Nafion and N-CHS composites.

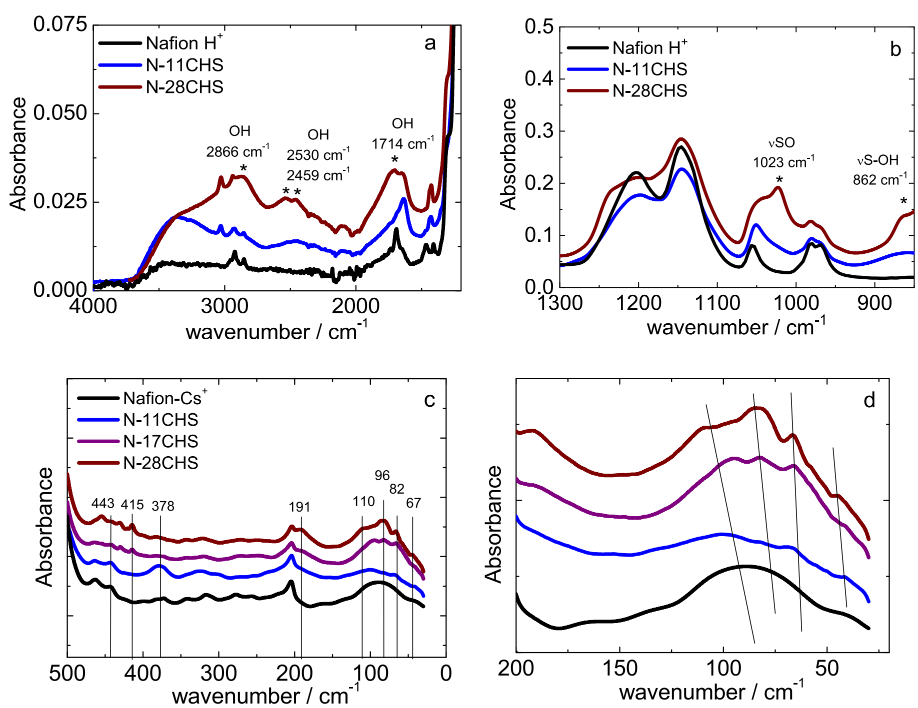

Fig. 6. Mid infrared (a and b, obtained in the ATR mode) and far infrared spectra (c and d in transmission mode) of Nafion and N-CHS composites under the low RH conditions (vacuum). In c and d, the spectra were vertically displaced for better visualization.

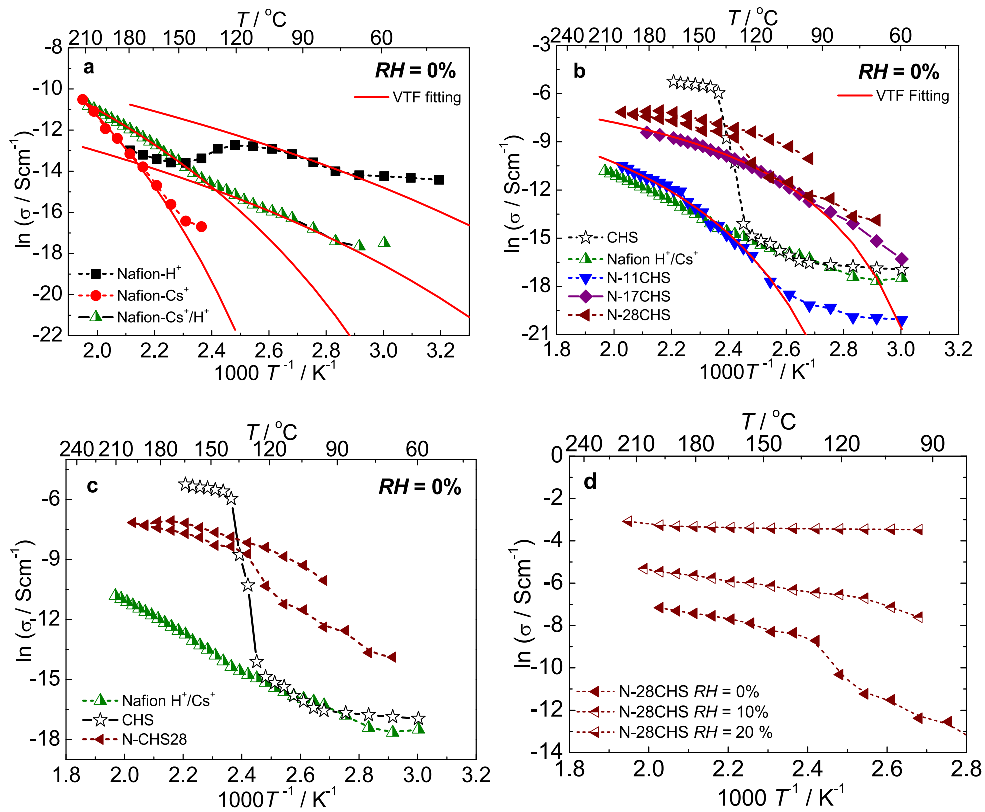

Fig. 8. Arrhenius plots for the ionic conductivities of reference samples (a); for the proton conductivity of CHS (b); for the ionic conductivities of N-11CHS, N-17CHS and N-28CHS (c) at anhydrous condition; and for the ionic conductivities of N-28CHS at different relative humidity.

~0.20 eV and T_0 of ~ −45 °C, which suggests that at low temperatures the proton motion is activated whereas at higher T the mixed proton and cesium conductivity takes place. It is possible that at low-T, the conductivity is dominated by the motion of proton ions, which can be confirmed with the fact that in the cesium conductivity of Nafion-Cs^+ sample only at $T > 160$ °C appreciable values of ionic conductivity were obtained. Moreover, the activation energy fitted for the low-T range is more characteristic of the proton transport. At high-T range, the higher activation energies fitted suggest that both proton and cesium transport take place. The fitted T_0 values evidence that the Nafion-Cs^+/H^+ is likely to possess two distinct glass transition temperatures.

Fig. 8b shows the superprotonic transition in the proton conductivity curve of the $CsHSO_4$ and the difference of the conductivity magnitude with respect to the reference sample Nafion-Cs^+/H^+. The conductivity of Nafion and CHS displays similar magnitude for $T < 100$ °C that is a critical temperature above which the proton conductivity of CHS increases several orders of magnitude, from $\sigma \sim 2 \times 10^{-8}$ Scm^{-1} ($T = 70$ °C) to $\sim 5 \times 10^{-3}$ Scm^{-1} ($T = 180$ °C). The conductivity of Nafion-Cs^+/H^+ displays a two order of magnitude improvement as it amounts to $\sigma \sim 3 \times 10^{-6}$ Scm^{-1} at $T = 180$ °C.

In Fig. 8b showing the ionic conductivities for the prepared nanocomposites the striking result can be immediately identified: whereas the ionic conductivity of composite N-11CHS is similar to Nafion-Cs^+/H^+ (at $T > 140$ °C), $\sigma \sim 3 \times 10^{-7}$ Scm^{-1}, the conductivity of both N-17CHS and N-28CHS increased to $\sigma \sim 4 \times 10^{-5}$ Scm^{-1} and $\sim 2 \times 10^{-4}$ Scm^{-1} at $T \sim 140$ °C, respectively, in excellent agreement with the SAXS plots that evidenced the percolation threshold of the inorganic network within the polymer matrix is reached for the composites prepared in DMSO solutions. Moreover, the composite N-28CHS displays the superprotonic conductivity transition with the onset at $T \sim 130$ °C (Fig. 8c). Such findings are in accordance with the far infrared analysis, which showed that the bulk properties of the CHS phase are evident in the N-28CHS sample. The VTF fittings for the composite conductivities are $E_a \sim 0.10$ eV and ~ 0.05 eV for N-11CHS, and both N-17CHS and N-28CHS, respectively, which strongly supports that primarily the transport of protons occurs within the composite samples, as it takes place in $CsHSO_4$. The extremely low E_a values observed for the composite materials indicate that the main conduction mechanism is Grotthuss, in agreement with the conduction mechanism reported for $CsHSO_4$ [7]. It is interesting to point out that the conductivity upon cooling displays a similar behavior than pristine CHS, *i.e.* the conductivity curve does not possess the abrupt drop upon cooling [43]. The absence of a sharp conductivity transition in N-17CHS may have its origin in the very small sizes of the CHS nanoparticles that are not sufficiently ordered structure (bulky) to provide the same transition observed for macroscopic $CsHSO_4$ phase. This interpretation is supported by the VTF temperature dependence of the conductivity exhibited by the composite samples, which is evidence that the proton transport within the $CsHSO_4$ follows the main and side chain modulation of the polymer phase. The measurement of the conductivity of N-28CHS upon cooling displays the VTF temperature dependence, which is further evidence that the conductivity of CHS inserted in Nafion has a strong dependence on the dynamics of the ionomer side chains. As such, the presence of the conductivity leap in N-28CHS helps in the investigation of the origins of the superproton conductivity in solid acids.

It is worth noting that the fact that the temperature dependence of the proton conductivity followed the VTF behavior supports that no significant leaching out of the CHS phase from the composite membrane occurs. The leaching out of the CHS phase from the composite would result in a deviation from the VTF behavior since it is strongly dependent on the sample composition.

One of the most important features of the composite material properties arises from the analysis of the temperature dependence of the conductivity displayed with respect to the reference samples. The viscoelastic properties of ionomers possess a Vogel-Tamman-Fulcher temperature dependence, *i.e.*, the main and side chain dynamics are a function of the glass transition temperature (T_g) following the modified Arrhenius temperature dependence: $\exp[-E_a(kT - kT_0)^{-1}]$, where E_a is the activation energy, k is Boltzmann constant, T_0 is the Vogel temperature and is usually 100 K lower than the actual T_g [9]. In this context, two possible temperature ranges are important: *i*) the composite material temperature, or operating temperature (T_{op}) is lower than T_0; and *ii*) the T_{op} is higher than T_0. In the first case, the composite is in the glassy state and the "static" polymer dynamics cannot affect the crystal structure of the inorganic phase. In the latter case, which is the focus in this study, the polymer is in the rubber state and the larger the difference $kT_{op} - kT_0$, the higher is the segmental motion energies of the main and side chains of the ionomer. Considering the glass transition temperatures of polyethylene and polytetrafluoroethylene-based ionomers [9], < -20 °C, and a T_{op} of 200 °C, the term $kT_{op} - kT_0$ reaches ~5 kJ.mol^{-1}, which is in the range of magnitude of the hydrogen bonding energies in the solid state that varies from ~0.8 to 160 kJ.mol^{-1} [18]. At high temperatures, the hosting organic matrix can perturb the hydrogen bonds within the crystal lattice of the inorganic phase. This interrelationship is maximized at the superprotonic conductivity transition temperature of the solid acid, when the hydrogen bonds are much weaker since there is a continuous breaking and restructuring of the hydrogen bonding involved in the proton conduction mechanism [14,19].

The T_0 for N-17CHS and N-28CHS is ~ +20 °C; the highest value observed, which is in good accordance with the stress-strain curves (Fig. 7). Such T_0 larger than that of the Nafion-Cs^+ may be a result of two factors: *i*) the presence of a large volume of nanoparticles; and *ii*) the restricted motion of the main and side chains due to the anchored side chains in the $CsHSO_4$ nanophase. In general, the composite Nafion-$CsHSO_4$ represents a genuine synergistic system in which both particle and added phase properties are affected by the mixture and the resulting property is not inherited from the individual phases. The conductivity value of ~10^{-5} to 10^{-4} Scm^{-1} ($T = 180$ °C) is too low to perform fuel cell measurements; however, the data obtained indicate that the N-CHS composites are promising materials to enhance the proton conduction properties of membranes for proton exchange membrane fuel cells as indicated in Fig. 8d. In Fig. 8d, it is shown that small increments in the relative humidity from 0 to 20% can boost the ion conductivity from 10^{-4} to 10^{-2} Scm^{-1}, a feature more pronounced in the low temperature range ($T < 120$ °C) limited by the Nafion conductivity. The experimental findings of the present study point towards promising strategies to further improve the proton conductivity of polymer-based composites. For example, the CsH_2PO_4 displays a superprotonic transition at 240 °C. As shown in this manuscript, Nafion in the cesium form has thermal stability to stand such high temperatures and by CsH_2PO_4 being less soluble in water, it may produce larger nanoparticles and enhance the solid acid bulky properties, and consequently the superproton conductivity, which are essential for future fuel cell tests.

4. Conclusion

The combined analyses of SAXS, FTIR, SEM-FEG, and EIS measurements confirm that the proton conductivity of Nafion-CHS composites is a result of the coupling dynamics of the CHS and polymer phases. SEM-FEG, SAXS, and FTIR data support that the solid acid phase exists within the ionic clusters of Nafion. Moreover, the CHS phase is percolated in the cluster network of Nafion for the samples prepared with the solvent DMSO. The electrical properties of the composite exhibited truly synergistic behavior in which the addition of solid acids into Nafion promoted a change in the polymer dynamics, as evidenced by the substantial change of the glass transition temperature. The interaction with the ionomer promoted a change in the mechanical and electrical properties of the inorganic phase as a result of the anchoring of the side chains into the CHS phase. The proton conductivity in anhydrous condition is substantially increased in Nafion-CHS composites with high concentration of the inorganic superprotonic conducting phase. The experimental results demonstrate the modulation of the proton conductivity of solid electrolyte composites based on ionomers and solid acids. Such synergistic composites open promising strategies to combine high conductivity and mechanical properties of each phase towards application.

CRediT authorship contribution statement

Bruno R. de Matos: Writing – review & editing, Writing – original draft, Visualization, Validation, Methodology, Investigation, Formal analysis, Data curation, Conceptualization. **Ulrich Schade:** Resources, Project administration, Funding acquisition, Data curation. **Ljiljana Puskar:** Writing – review & editing, Investigation, Funding acquisition, Formal analysis, Data curation. **Elisabete I. Santiago:** Writing – review & editing, Project administration, Funding acquisition, Formal analysis. **Fabio C. Fonseca:** Writing – review & editing, Supervision, Resources, Project administration, Investigation, Funding acquisition.

Declaration of competing interest

The authors declare that they have no known competing financial interests or personal relationships that could have appeared to influence the work reported in this paper.

Acknowledgements

The authors are grateful for the support of the Brazilian National Council for Scientific and Technological Development (CNPq) initiatives Sis-H2 (CNPq grant n. 407967/2022-2) and IBH2-MCTI (CNPq grant n. 405793/2022-7); Fundação de Amparo à Pesquisa do Estado de São Paulo (FAPESP) grants n. 2024/00989-7, 2022/07786-9, and 2023/14931-8. FCF and EIS are CNPq fellows. SAXS measurements were performed at Laboratório Nacional de Luz Síncrotron (LNLS) under the proposal n° 18801. FTIR experiments were carried out on the IRIS beamline, BESSY II synchrotron at Helmholtz-Zentrum Berlin für Materialien und Energie, Berlin, Germany (HZB proposal 18207430-ST). Authors are thankful to Dr. S. G. M. Carvalho and Dr. H. A. Zen for their assistance with the SEM-FEG and stress-strain measurements, respectively.

Data availability

Data will be made available on request.

References

[1] O. Kim, K. Kim, U.H. Choi, M.J. Park, Tuning anhydrous proton conduction in single-ion polymers by crystalline ion channels, Nature Comm. 9 (2018) 5029.
[2] B. Schumm, A. Dupuy, M. Lux, C. Girsule, S. Dörfler, F. Schmidt, M. Fiedler, M. Rosner, F. Hippauf, S. Kaskel, Dry battery electrode technology: from early concepts to industrial applications, Adv. Energy Mater. 15 (2025) 2406011.
[3] M. Eikerling, A. Kulikovsky, Polymer Electrolyte Fuel Cell, CRC Press, 2017.
[4] M.F.H. Schuster, W.H. Meyer, Anhydrous proton-conducting polymer, Annu. Rev. Mater. Res. 33 (2003) 233.
[5] M. Yamada, I. Honma, An anhydrous proton conductor based on lactam-Lactim tautomerism of uracil, Chem. Phys. Chem. 5 (2004) 724–728.
[6] S. Fop, R. Vivani, S. Masci, M. Casciola, A. Donnadio, Anhydrous superprotonic conductivity in the zirconium acid triphosphate ZrH5(PO4)3, Angew. Chem. Int. Ed. 62 (2023) e202218421.
[7] S.M. Haile, D.A. Boysen, C.R.I. Chisholm, R.B. Merle, Solid acids as fuel cell electrolytes, Nature 410 (2001) 910–913.
[8] D.A. Boysen, T. Uda, C.R.I. Chisholm, S.M. Haile, Performance solid acid fuel cells through humidity stabilization, Science 303 (2004) 68–70.
[9] S.J. Osborn, M.K. Hassan, G.M. Divoux, D.W. Rhoades, K.A. Mauritz, R.B. Moore, Glass transition temperature of perfluorosulfonic acid ionomers, Macromolecules 40 (2007) 3886–3890.
[10] J.E. Mark, C.Y.-C. Lee, P.A. Bianconi, Hybrid Organic-Inorganic Composites. ACS Symposium Series, vol. 585, American Chemical Society, Washington, DC, 1995.
[11] Q. Deng, R.B. Moore, K.A. Mauritz, Novel Nafion/ORMOSIL hybrids via in situ sol-gel reactions. 1. Probe of ORMOSIL phase nanostructures by infrared spectroscopy, Chem. Mater. 7 (1995) 2259–2268.

[12] D. Truffier-Boutry, A. De Geyer, L. Guetaz, O. Diat, G. Gebel, Structural study of zirconium phosphate−Nafion hybrid membranes for high-temperature proton exchange membrane fuel cell applications, Macromolecules 40 (2007) 8259–8264.

[13] B.R. Matos, C.A. Goulart, B. Tosco, J.S. da Silva, R.A. Isidoro, E.I. Santiago, M. Linardi, U. Schade, L. Puskar, F.C. Fonseca, A.C. Tavares, Properties and DEFC tests of nafion - functionalized titanate nanotubes composite membranes prepared by melt-extrusion, J. Membr. Sci. 604 (2020) 118042.

[14] A. Goni-Urtiaga, D. Presvytes, K. Scott, Solid acids as electrolyte materials for proton exchange membrane (PEM) electrolysis: review, Int. J. Hydrog Energ. 37 (2012) 3358–3372.

[15] B.R. Matos, R.A. Isidoro, E.I. Santiago, F.C. Fonseca, Performance enhancement of direct ethanol fuel cell using nafion composites with high volume fraction of titania, J. Power Sources 268 (2014) 706–711.

[16] S.K. Young, K.A. Mauritz, Dynamic mechanical analyses of nafion®/organically modified silicate nanocomposites, J. Polym. Sci. Part B. Polym. Phys. 39 (2001) 1282–1295.

[17] A. D'Epifanio, M.A. Navarra, F.C. Weise, B. Mecheri, J. Farrington, S. Licoccia, S. Greenbaum, Composite Nafion/sulfated zirconia membranes: effect of the filler surface properties on proton transport characteristics, Chem. Mater. 22 (2010) 813–821.

[18] T. Steiner, The hydrogen bond in the solid state, Angew. Chem. 41 (2002) 48–76.

[19] C.R.I. Chisholm, Y.H. Jang, S.M. Haile, W.A. Goddard III, Superprotonic phase transition of $CsHSO_4$: a molecular dynamics simulation study, Phys. Rev. B 72 (2005) 134103.

[20] M. Amirinejad, S.S. Madaeni, E. Rafiee, S. Amirinejad, Cesium hydrogen salt of heteropolyacids/Nafion nanocomposite membranes for proton exchange membrane fuel cells, J. Membr. Sci. 377 (2011) 89–98.

[21] W. Wu, Z. Zhou, Y. Wang, Y. Zhang, Y. Wang, J. Wang, Y. Zou, Manipulating the ionic nanophase of nafion by in situ precise hybridization with polymer quantum dot towards highly enhanced fuel cell performances, Nanoresearch 15 (2022) 4124.

[22] Z. Zhou, Y. Wang, J. Lin, Y. Zhang, L. Qu, W. Wu, J. Wang, In-situ molecular-level hybridization enabling high-sulfonation-degree sulfonated poly(ether ether ketone) membrane with excellent anti-swelling ability and proton conduction, Int. J. Hydrog Energ. 46 (2021) 31312.

[23] W. Wu, Y. Li, J. Liu, J. Wang, Y. He, K. Davey, S.-Z. Qiao, Molecular-level hybridization of nafion with quantum dots for highly enhanced proton conduction, Adv. Mater. 30 (2018) 1707516.

[24] D.S. McLachlan, M. Blaszkiewicz, R.E. Newnham, Electrical resistivity of composites, J. Am. Ceram. Soc. 73 (1990) 2187.

[25] K.A. Mauritz, M.K. Hassan, Nanophase separated perfluorinated ionomers as sol-gel polymerization templates for functional inorganic oxide nanoparticles, Polym. Rev. 47 (2007) 543.

[26] B.R. Matos, E.I. Santiago, R. Muccillo, I.A. Velasco-Davalos, A. Ruediger, A. C. Tavares, F.C. Fonseca, Interplay between α-relaxation and morphology transition of perfluorosulfonate ionomer membranes, J. Power Sources 293 (2015) 859–867.

[27] B.R. Matos, J.S. da Silva, E.I. Santiago, D.F. Parra, D.J. Carastan, D.Z. de Florio, H. E. Andrada, A.C. Carreras, F.C. Fonseca, Proton and cesium conductivity in perfluorosulfonate ionomers at low and high relative humidity, Solid State Ionics 301 (2017) 86–94.

[28] J. Baran, M.K. Marchewka, Vibrational investigation of phase transitions in $CsHSO_4$ crystal, J. Mol. Struct. 614 (2002) 133–149.

[29] J. Baran, Polarized infrared and Raman spectra of a CsHSO4 single crystal, J. Mol. Struct. 162 (1987) 211–228.

[30] K.-D. Kreuer, G. Portale, A critical revision of the nano-morphology of proton conducting ionomers and polyelectrolytes for fuel cell applications, Adv. Funct. Mater. 23 (2013) 5390–5397.

[31] J.S. da Silva, S.G.M. Carvalho, R.P. da Silva, A.C. Tavares, U. Schade, L. Puskar, F. C. Fonseca, B.R. Matos, SAXS signature of the lamellar ordering of ionic domains of perfluorinated sulfonic-acid ionomers by electric and magnetic field-assisted casting, Phys. Chem. Chem. Phys. 22 (2020) 13764–13779.

[32] S.K. Young, S.F. Trevino, N.C. Beck Tan, Small-angle neutron scattering investigation of structural changes in nafion membranes induced by swelling with various solvents, J. Polym. Sci. B Polym. Phys. 40 (2002) 387.

[33] A. Eisenberg, H. Yeager, Perfluorinated ionomer membranes, in: ACS Symposium Series 180, American Chemical Society, Washington, DC, 1982.

[34] L. Rubatat, A.L. Rollet, G. Gebel, O. Diat, Evidence of elongated polymeric aggregates in Nafion, Macromolecules 35 (2002) 4050–4055.

[35] B.R. Matos, E.I. Santiago, J.F.Q. Rey, F.C. Fonseca, Origin of α and β relaxations of Nafion, Phys. Rev. E 89 (2014) 052601.

[36] S.R. Lowry, K.A. Mauritz, An investigation of ionic hydration effects in perfluorosulfonate ionomers by Fourier transform infrared spectroscopy, J. Am. Chem. Soc. 102 (1980) 4665–4667.

[37] L. Puskar, E. Ritter, U. Schade, M. Yandrasits, S.J. Hamrock, M. Schaberg, E.F. Aziz, Infrared dynamics study of thermally treated perfluoroimide acid proton exchange membranes, Phys. Chem. Chem. Phys. 19 (2017) 626–635.

[38] M. Pham-Thit, Ph. Colomban, A. Novak, R. Blinc, Vibrational spectra of and phase transitions in caesium hydrogen sulphate, J. Raman Spectrosc. 18 (1987) 185–194.

[39] Y. Kawano, Y. Wang, R.A. Palmer, S.R. Aubuchon, Stress-strain curves of Nafion membranes in acid and salt forms, Polímeros: Ciência e Tecnologia 12 (2002) 96–101, https://doi.org/10.1590/S0104-14282002000200008.

[40] B.R. Caire, M.A. Vandiver, T.P. Pandey, A.M. Herring, M.W. Liberatore, Accelerated mechanical degradation of anion exchange membranes via hydration cycling, J. Electrochem. Soc. 163 (2016) H964–H969.

[41] J.J. Fontanella, M.G. Mclin, M.C. Wintersgill, Electrical relaxation in in situ dried acid-form Nafion, J. Polym.Sci. Part B: Polym. Phys. 32 (1994) 501.

[42] B.R. Matos, The genuine *ac*-to-*dc* proton conductivity crossover of Nafion and polymer dielectric relaxations as a fuel cell polarization loss, J. Electroanal. Chem. 871 (2020) 114357.

[43] A.I. Baranov, L.A. Shuvalov, N.M. Shchagina, Superion conductivity and phase transitions in $CsHSO_4$ and $CsHSeO_4$ crystals, J. Exper. Theoret. Phys. Lett. 36 (1982) 459.